AD_____

Award Number: ÖOET ÖFÏ ËEH ËFË ËÍ FÍ

TITLE: Û˘ æ} cãæcãç^ÁOÈ æ^•ãÁ¸-ÁÔæ}&^¦ÁÔ^||ÁТ ãˆ¦æcæ]}Á§¸ÁÕ¦æåãˆ^o¸Á¸-ÁÒÕØÊ¸ PÕØÊæ}åÁ ÙÖØÊæ]@æ√•ã*ÆæТ æ&[¦˘ã̃ã&Á@{[æcãÁÖ^çã&^

PRINCIPAL INVESTIGATOR: ÁP[[ŠãR^[}ÁŠÚ@ÖÈ

CONTRACTING ORGANIZATION: V@ÁÑj ̃ç^•ãÁ¸-ÁÔæå[¦}ãæ
Qjçã}^ÊÁÔOÆÁÃGÏJÏÁ

REPORT DATE: Jæ}˘æ^ÁG€€Í

TYPE OF REPORT: Øã}æ|

PREPARED FOR: U.S. Army Medical Research and Materiel Command
Fort Detrick, Maryland 21702-5012

DISTRIBUTION STATEMENT: Approved for public release; distribution unlimited

The views, opinions and/or findings contained in this report are those of the author(s) and should not be construed as an official Department of the Army position, policy or decision unless so designated by other documentation.

REPORT DOCUMENTATION PAGE				*Form Approved* OMB No. 0704-0188

Public reporting burden for this collection of information is estimated to average 1 hour per response, including the time for reviewing instructions, searching existing data sources, gathering and maintaining the data needed, and completing and reviewing this collection of information. Send comments regarding this burden estimate or any other aspect of this collection of information, including suggestions for reducing this burden to Department of Defense, Washington Headquarters Services, Directorate for Information Operations and Reports (0704-0188), 1215 Jefferson Davis Highway, Suite 1204, Arlington, VA 22202-4302. Respondents should be aware that notwithstanding any other provision of law, no person shall be subject to any penalty for failing to comply with a collection of information if it does not display a currently valid OMB control number. **PLEASE DO NOT RETURN YOUR FORM TO THE ABOVE ADDRESS.**

1. REPORT DATE *(DD-MM-YYYY)* 01-01-2005	2. REPORT TYPE Final	3. DATES COVERED *(From - To)* 1 JUL 2003 - 31 DEC 2004

4. TITLE AND SUBTITLE Quantitative Analysis of Cancer Cell Migration in Gradients of EGF, HGF, and SDF-alpha Using a Microfluidic Chemotaxis Device	5a. CONTRACT NUMBER
	5b. GRANT NUMBER DAMD17-03-1-0515
	5c. PROGRAM ELEMENT NUMBER
6. AUTHOR(S) Noo Li Jeon, Ph.D. E-Mail: nljeon@gmail.com	5d. PROJECT NUMBER
	5e. TASK NUMBER
	5f. WORK UNIT NUMBER

7. PERFORMING ORGANIZATION NAME(S) AND ADDRESS(ES) The University of California Irvine, CA 92697	8. PERFORMING ORGANIZATION REPORT NUMBER

9. SPONSORING / MONITORING AGENCY NAME(S) AND ADDRESS(ES) U.S. Army Medical Research and Materiel Command Fort Detrick, Maryland 21702-5012	10. SPONSOR/MONITOR'S ACRONYM(S)
	11. SPONSOR/MONITOR'S REPORT NUMBER(S)

12. DISTRIBUTION / AVAILABILITY STATEMENT
Approved for Public Release; Distribution Unlimited

13. SUPPLEMENTARY NOTES

14. ABSTRACT

We continued to develop microfluidic chambers to study breast cancer cell chemotaxis as it relates to metastasis. As part of this effort, we developed 3D culture devices that can generate concentration gradients of soluble factors in 3D gels, allowing cancer cell migration to be investigated in physiologically relevant conditions. We first developed devices capable of generating linear and non-linear gradients in 3D collagen gels. We then implemented these devices and developed a co-culture model to study the interaction between breast cancer cells and macrophages, each cultured in a distinct extracellular matrix that better simulates tissue composition. We studied the migration of these different cell types in these 3D devices. These studies suggested an intriguing synergy between tumor cells and immune cells, and pave the way for complex studies of cancer cell behavior in in vitro models that can better mimic tumor and tissue microenvironments.

15. SUBJECT TERMS
Cell Migration, Chemotaxis, Metastasis, Microfabrication, 3D co-cultures

16. SECURITY CLASSIFICATION OF:			17. LIMITATION OF ABSTRACT	18. NUMBER OF PAGES	19a. NAME OF RESPONSIBLE PERSON USAMRMC
a. REPORT U	b. ABSTRACT U	c. THIS PAGE U	UU	18	19b. TELEPHONE NUMBER *(include area code)*

Standard Form 298 (Rev. 8-98)
Prescribed by ANSI Std. Z39.18

Table of Contents

Introduction

This report describes our recent accomplishments in the development of microfluidic devices for the study of breast cancer cell chemotaxis. We have previously 2D devices for the study of breast cancer cell chemotaxis on fat surfaces. We now report on development of 3D devices that produce concentration gradients scaffolds of extracellular matrix proteins, allowing cancer cell migration to be investigated in physiologically relevant conditions. We first developed devices capable of generating linear and non-linear gradients in 3D collagen gels. We then implemented these devices and developed a co-culture model to study the interaction between breast cancer cells and macrophages, each cultured in a distinct extracellular matrix that better simulates tissue composition.

Body

We developed devices that generate complex (linear and nonlinear) gradients in 3D gels by free diffusion between the source and sink main channels. Linear gradients are generated when the boundary conditions are such that the molecular flux area is constant across the diffusion region, as in a straight channel. In order to generate nonlinear profiles that are more relevant for both chemical and biological conditions, the flux area needs to differ across the diffusion region. This was achieved by fabricating either an array of discrete microchambers, or a continuous channel with openings at the interface of the diffusions region to the source and sink channels.

We also developed devices that allow different 3D gels to be patterned in a controlled manner, enabling different cells to be cultured in different gels side by side.

4

The utility of this system for multicellular 3D cultures was demonstrated by investigating the behaviors of metastatic breast cancer cells and tumor-derived macrophages in spatially well-defined geometries. In these experiments, distinct phenotypes were exhibited by the macrophages when cultured next to the tumor cells, possibly due to paracrine signals that diffuse between adjacent gel channels.

Key Research Accomplishments

- Developed 3D culture devices capable of generating complex linear and nonlinear gradients of soluble factors in 3D gels
- Developed a 3D co-culture device that allows different gels to be patterned with controlled geometries, and produce stable concentration gradients through these gels
  - Demonstrated the utility of these devices in studying the invasion of macrophages into the extracellular matrix surrounding cancer cells, mimicking the behavior of these different cell types *in vivo*

Reportable Outcomes

Manuscripts:

- Mosadegh B, Huang C, Park JW, Shin HS, Chung BG, Hwang SK, Lee KH, Kim HJ, Brody J, Jeon NL. Generation of stable complex gradients across two-dimensional surfaces and three-dimensional gels. *Langmuir,* 2007, **23** (22), 10910-10912. (Attached in Appendix)

- Huang CP, Lu J, Seon H, Lee AP, Flanagan LA, Kim HY, Putnam AJ, Jeon NL. Engineering microscale cellular niches for three-dimensional multicellular co-cultures. *Lab On A Chip,* 2009, **9** (12), 1740-1748. (Attached in Appendix)

<u>Conclusions</u>

We developed devices capable of generating linear and non-linear gradients in 3D collagen gels. We then implemented these devices and developed a co-culture model to study the interaction between breast cancer cells and macrophages, each cultured in a distinct extracellular matrix that better simulates tissue composition. We studied the migration of these different cell types in these 3D devices. These studies suggested an intriguing synergy between tumor cells and immune cells, and pave the way for complex studies of cancer cell behavior in *in vitro* models that can better mimic tumor and tissue microenvironments.

<u>References</u>

Mosadegh B, Huang C, Park JW, Shin HS, Chung BG, Hwang SK, Lee KH, Kim HJ, Brody J, Jeon NL. Generation of stable complex gradients across two-dimensional surfaces and three-dimensional gels. *Langmuir,* 2007, **23** (22), 10910-10912. (Attached in Appendix)

Huang CP, Lu J, Seon H, Lee AP, Flanagan LA, Kim HY, Putnam AJ, Jeon NL. Engineering microscale cellular niches for three-dimensional multicellular co-cultures. *Lab On A Chip,* 2009, **9** (12), 1740-1748. (Attached in Appendix)

Generation of Stable Complex Gradients Across Two-Dimensional Surfaces and Three-Dimensional Gels

Bobak Mosadegh,[†] Carlos Huang,[†] Jeong Won Park,[†] Hwa Sung Shin,[†] Bong Geun Chung,[†] Sun-Kyu Hwang,[‡] Kun-Hong Lee,[‡] Hyung Joon Kim,[†] James Brody,[†] and Noo Li Jeon*,[†]

Department of Biomedical Engineering, University of California, Irvine, 3109 Natural Sciences 2, Irvine, California 92697-2715, and Department of Chemical Engineering, Pohang University of Science and Technology (POSTECH), San 31, Hyoja-Dong, Nam-Gu, Pohang, Gyeongbuk, South Korea 790-784

Many chemical and biological processes are dependent on molecular gradients. We describe a new microfluidic approach that can be used to produce spatiotemporal gradients across two-dimensional surfaces and three-dimensional gels under flow-free conditions. Free diffusion between dynamically replenished flow channels acting as a sink and source is utilized to give rise to stable steady-state gradient profiles. The gradient profile is dictated by the engineered design of the device's gradient-generating region. Different designs can yield both linear and non-linear gradients of varying profiles. More complex gradients can be made by juxtaposing different designs within a single gradient-generating region. By fabricating an array of designs along the gradient-generating region, different gradient profiles can be generated simultaneously, allowing for parallel analysis. Additionally, simple methods of localizing gels into microdevices are demonstrated. The device was characterized by experimentally obtained gradient profiles of fluorescent molecules that corroborated closely with a simulated finite element model.

A wide range of chemical and biological phenomena are influenced by gradients of molecular species.[1–4] Recent progress in microfabrication and microfluidics has resulted in innovative approaches to generate and maintain spatial and temporal gradients.[5–9] Two general approaches have been described: (1) forming gradients perpendicular to continuously flowing streams of varying concentration and (2) forming gradients along a channel by free-diffusion between a source and a sink. The first method is advantageous for producing stable complex gradients,[10] but the constant flow and shear stress are not compatible with experiments such as crystallization and chemotaxis of non-adherent or weakly adherent cells (i.e., bacterial and yeast). Although the constant flow can maintain uniform growth factor conditions, it can also introduce unwanted perturbations to autocrine/paracrine factors for cell signaling investigations. To overcome some of these drawbacks, several approaches have utilized free diffusion to produce gradients in static environments.[5–9] However, because they rely on free diffusion, the gradient profile changes with time, and it is difficult to obtain a steady-state gradient over long periods. In addition, the shape of the gradient profiles that can be generated is limited, and it

has not been possible to generate gradients across three-dimensional (3D) environments.

This paper describes the design and characterization of a monolithic microfluidics-based device that can generate an array of complex steady-state soluble molecular gradients in flow-free two-dimensional (2D) and 3D environments. 3D hydrogels are increasingly used in the investigation of many cell behaviors[11,12] as they simulate in vivo conditions better than 2D models. Investigations on the invasive migration of metastatic cancer cells and stem cell niches can benefit greatly if complex, stable molecular gradients can be achieved across 3D gels in flow-free conditions. Figure 1A,B shows two examples of the device, fabricated in poly(dimethylsiloxane) (PDMS)[13] that generates gradients across 2D surfaces and 3D gels, respectively. The design consists of two distinct regions: (1) two parallel main channels that act as the source and sink that are continuously replenished by flow and (2) a gradient-generating region (GGR) located between the source and sink channels. This principle can be applied to build more complex profiles by simply engineering the shape of the GGR. Continuously replenished source and sink are advantageous over static reservoirs because their concentration can be kept constant, and thus the gradients can be maintained at a constant profile in steady-state.

The device generates gradients across the GGR by free-diffusion between the source and sink main channels. For gradients over 2D surfaces, convective flow into the GGR is minimized by designing the height of the GGR (3 μm) to be significantly smaller than that of the main channels (100 μm). The large difference in GGR channel height yields an even larger difference in fluidic resistance, causing flow to take the path of least resistance (main channel) rather than entering the GGR, allowing only diffusive transport. Additionally, post structures can be fabricated along the interface of the GGR and main channels to provide additional resistance when large openings are needed

* Corresponding author.

[†] University of California, Irvine.

[‡] POSTECH.

(1) Maheshwari, G.; Wells, A.; Griffith, L. G.; Lauffenburger, D. A. *Biophys. J.* **1999**, *76*, 2814–2823.

(2) Yang, X.; Corvalan, J.; Wang, P.; Roy, C. M.; Davis, C.G. *J. Leukocyte Biol.* **1999**, *66*, 401–410.

(3) Condeelis, J. S.; Wyckoff, J. B.; Bailly, M.; Pestell, R.; Lawrence, D.; Backer, J.; Segall, J. E. *Semin. Cancer Biol.* **2001**, *11*, 119–128.

(4) Yu, H.; Meyvantsson, I.; Shkel, A.; Beebe, D. J. *Lab Chip* **2005**, *5*, 1089–1095.

(5) Abhyankar, V. V.; Lokuta, M. A.; Huttenlocher, A.; Beebe, D. J. *Lab Chip* **2006**, *6*, 389–393.

(6) Wu, H.; Huang, B.; Zare, R. N. *J. Am. Chem. Soc.* **2006**, *128*, 4194–4195.

(7) Keenan, T. M.; Hsu, C. H.; Folch, A. *Appl. Phys. Lett.* **2006**, *89*, 114103–114105.

(8) Saadi, W.; Rhee, S. W.; Lin, F.; Chung, B. G.; Vahidi, B.; Jeon, N. L. *Biomed. Microdevices* **2007**, *9*, 627–635.

(9) Paliwal, S.; Iglesias, P. A.; Campbell, K.; Hilioti, Z.; Groisman, A.; Levchenko, A. *Nature* **2007**, *1038*, 05561.

(10) Jeon, N. L.; Baskaran, H.; Dertinger, S. K. W.; Whitesides, G. M.; Van de Water, L.; Toner, M. *Nat. Biotechnol.* **2002**, *20*, 826–830.

(11) Wolf, K.; Friedl, P. *Br. J. Dermatol.* **2006**, *154*, 11–5.

(12) Hartmann, A.; Boukamp, P.; Friedl, P. *Blood Cells, Mol. Dis.* **2006**, *36*, 191–193.

(13) Wu, H.; Odom, D. T.; Whitesides, G. M. *J. Am. Chem. Soc.* **2003**, *125*, 554–559.
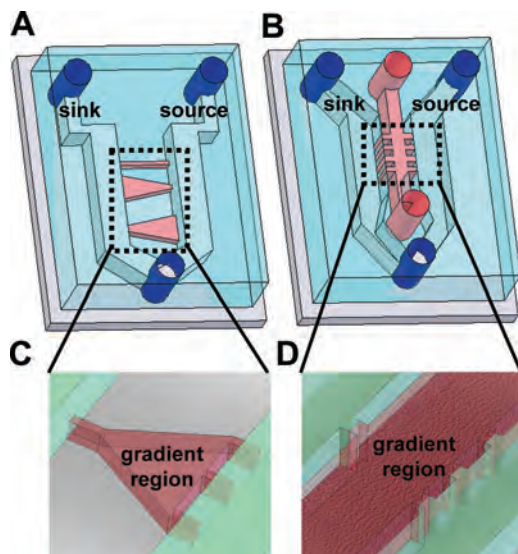
Figure 1. (A,B) Schematic of PDMS device with red region designating GGR and blue highlighting flow inlets and outlet: (A) GGR is a set of microchambers designed for gradients across a 2D surface; (B) GGR is a continuous channel with posts at the interface with main channels for gradients across a 3D gel. (C) Close-up of microchamber in a 2D surface gradient with posts at the interface of the GGR and the tapered microchamber to produce a nonlinear gradient. (D) Close-up of GGR for a 3D gel gradient with asymmetric posts designed to produce a nonlinear gradient.

for nonlinear gradient profiles, as shown in Figure 1C. A similar approach can be used to generate gradients across 3D gels, as shown in Figure 1D (see Supporting Information for photomicrograph of selectively filled GGR). This approach allows equal heights of the main channel and GGR by selectively filling the GGR with a 3D matrix (i.e., collagen gel), which increases the fluidic resistance, minimizing flow penetration into the GGR region. Additionally, the gel can also facilitate the 3D environments for cell biology applications.

Linear gradients are generated when the boundary conditions are such that the molecular flux area is constant across the GGR, as in a straight channel.[5,9] In order to generate nonlinear profiles that are more relevant for both chemical and biological conditions,[14] the flux area needs to differ across the GGR. This was achieved by two different methods, which can be used for either 2D surfaces or 3D gels: (1) an array of discrete microchambers (Figure 1A) and (2) a continuous channel with openings at the interface of the GGR (Figure 1B) to the source and sink channels. For the first method, the gradient profile of each microchamber is determined by two factors: the geometric design of the microchamber and the relative openings to the source and sink. Linear profiles are produced for a straight channel, where slope depends on the length of the GGR. Nonlinear profiles are produced in an asymmetric design by tapering the microchamber, which causes a continual imbalance of the in-flux and out-flux area between the source and sink channels through which molecules diffuse. The degree of nonlinearity can also be changed (albeit slightly) by curved microchambers as compared to the straight tapering shown in Figure 1C. The second factor, which is relevant for both methods, is the ratio of the number of sink to source openings (area of GGR through which molecules diffuse). Linear gradients are produced when the openings are symmetric and evenly distributed at opposite ends since the in-flux and out-flux areas of the diffusing molecules are equal.
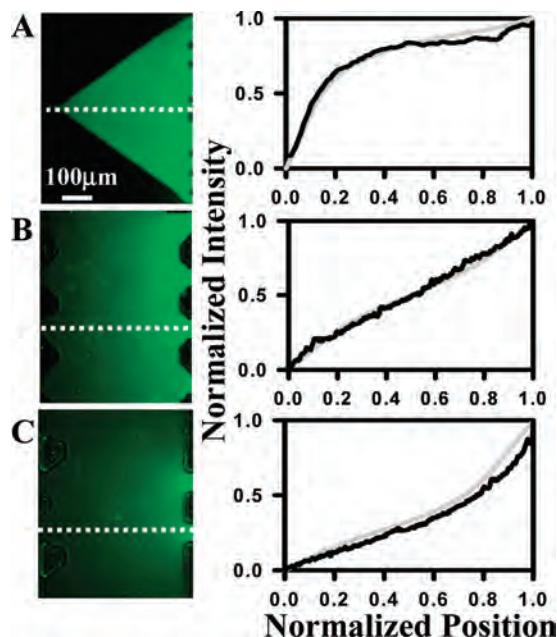
(14) Wang, S. J.; Saadi, W.; Lin, F.; Nguyen, C. M.; Jeon, N. L. *Exp. Cell Res.* **2004,** *1,* 180−189.

Figure 2. Fluorescent images and corresponding experimental (black) and theoretical (gray) gradient profiles across a GGR; intensity profiles taken across the white dash line. (A) 2D chamber shown in Figure 1A was used to produce a concave down nonlinear profile. The microchamber was 400 μm wide with openings 30 μm wide. (B) Gradients across 3D Matrigel were produced using the design shown in Figure 1B. Linear profiles were produced by designing the same number of openings to source and sink channels. (C) Mismatched number of openings to source (2) and sink (5) channels, resulting in a nonlinear profile. The openings were 50 μm wide.

Nonlinear gradients are produced when the number of openings are unbalanced, causing an unequal in-flux and out-flux area in the GGR. The degree of nonlinearity can be enhanced by increasing the ratio of openings and shortening the width of the GGR. For both methods, the gradient range is controlled by the concentrations of the source and sink, which can be further controlled temporally by switching the inlet solutions.

More complex gradient profiles can be made by a serial combination of different microchamber designs within one GGR. For example, juxtaposing a concave down and concave up nonlinear profile will yield a sigmoidal gradient profile (see Supporting Information). For the first method, this is achieved by having a "bow-tie"-shaped microchamber with wide openings to the source and sink channels that tapers toward the middle. For the second method, this is achieved by the same principle where two GGR regions have many openings to the source and sink channels on the outer sides but few connecting openings in the middle. Additionally, since various types of microchamber and post designs can be integrated during fabrication (see Supporting Information), a variety of both linear and nonlinear profiles can be generated on a single device for high-throughput experiments.

Shown in Figure 2 are three fluorescent micrographs and their corresponding experimental (black) and theoretical (gray) gradient profiles. The theoretical data was generated by a finite element modeling program under diffusion (see Supporting Information). The fluorescence gradient profiles were generated by infusing fluorescein into the right main channel (source) and deionized water into the left main channel (sink). Figure 2A is a concave down nonlinear gradient across a 400 μm tapering microchamber generated by having a large number of openings (11) to the source channel and a small number of openings (1) to the sink channel. Figure 2B,C shows gradients generated across a 3D

Matrigel. Figure 2B has symmetric and evenly distributed post structures, as in Figure 1B, yielding a linear gradient. Figure 2C has a mismatched number of openings (2 source and 5 sink), producing a nonlinear profile. Steady-state gradient profiles are stably maintained as long as no disruption occurs in the continual flow of solutions through the main channels (see Supporting Information).

We used two different methods (depending on the device design) to selectively localize the gels in the GGR (see Supporting Information). For devices with microchamber design (Figure 1A), the entire device was first filled with liquid gel followed by rapid aspiration with a house vacuum. Since the resistance across the GGR is considerably higher than that across the main channels, the gels in the GGR region were selectively left behind. The second method requires simple loading of liquid gel into the GGR inlet and can be used with the design shown in Figure 1B. To achieve reproducible results, the post structures (size and spacing) and surface properties of the device were optimized. After plasma treatment and bonding, channel surfaces were allowed to revert back to a hydrophobic state before the gel was injected into the GGR. The gel was confined to the GGR by surface tension until it solidified and then was used for gradient experiments. A number of gel materials such as collagen type I, Matrigel, and fibrin were successfully polymerized in the device using both methods.

This paper describes a microfluidic device capable of generating stable complex gradients across 2D surfaces and 3D gels in flow-free conditions. Two different designs and methods for generating selectively localized gels in micron-size channels have been developed. The ability to generate precise gradients in flow-free conditions and design different profiles by engineering the GGR chamber and placing them in series will be useful in a number of chemical (i.e., crystallization) and biological (i.e., tissue engineering and chemotaxis) experiments.

Engineering microscale cellular niches for three-dimensional multicellular co-cultures†

Carlos P. Huang,[a] Jente Lu,[ac] Hyeryung Seon,[b] Abraham P. Lee,[a] Lisa A. Flanagan,[c] Ho-Young Kim,[d] Andrew J. Putnam[ab] and Noo Li Jeon[*d]

Modeling the *in vivo* microenvironment typically involves placing cells in a three-dimensional (3D) extracellular matrix (ECM) in physiologically relevant context with respect to other cells. The mechanical and chemical features of 3D microenvironments play important roles in tissue engineering, tumor growth and metastasis, and in defining stem cell niches, and it is increasingly recognized that cells behave much differently when surrounded by a 3D ECM than when anchored to a 2D substrate. To create microenvironments that more closely mimic *in vivo* settings, here we describe a novel microfluidic device that allows multiple discrete constructs of 3D cell-laden hydrogels to be patterned in a sequence of simple steps. The microfluidic platform allows for real-time imaging of the interactions between multiple cell types exposed to both autocrine and paracrine signaling molecules, all within a 3D ECM environment. Detailed modeling determined that surface tension, hydrophobic interactions, and spatial geometry were important factors in containing the gels within distinct separate channels during the filling process. This allowed us to pattern multiple gel types side-by-side and pattern 3D gels spatially with tight dimensional control. Cells embedded in gels could be patterned by culturing MDA-MB-231 metastatic breast cancer cells and RAW 264.1 macrophage cells within distinct collagen type I and Matrigel ECM environments, respectively. Over a 7 day culture experiment, RAW cells invaded into neighboring gels containing MDA-MB-231 cells, but not into gels lacking cells. These studies demonstrate the versatility and potential of this new microfluidic platform to engineer 3D microscale architectures to investigate cell–cell and cell–matrix interactions.

Introduction

Driven in part by independent research efforts in the fields of tissue engineering and cancer, there is an increased emphasis to move cell biology away from homotypic two dimensional cell cultures towards three dimensional (3D) multicellular culture studies.[1–4] Multicellularity and three-dimensionality have both been shown to be important features of the microenvironment that can influence cell function.[1,2,4] In the body, 3D microenvironments not only surround most cells and provide a scaffolding structure with which these cells interact, they also involve multiple cell types that interact directly *via* heterotypic cell–cell junctions or *via* paracrine-mediated signaling mechanisms. Nevertheless, the ability to study these types of interactions in well-controlled 3D culture systems remains a challenge.

There are many examples in which multicellular culture systems have been used to provide physiologic cues and reveal insights into how cells may behave *in vivo*. For example, hepatocytes were shown to be more viable and retain their differentiated phenotype when cultured in the presence of 3T3 fibroblasts.[5] Embryonic stem cells are typically grown on a monolayer of irradiated fibroblasts to provide nutrients and paracrine factors that maintain pluripotency and support growth.[6]

In tumor biology specifically, the metastatic spread of cancer cells involves a dynamic interaction and remodeling of the microenvironment that is often facilitated by other cell types present in the surrounding stroma. It was recently reported that the invasion of carcinoma cells is enhanced when cultured with stromal fibroblasts, and that the tumor cells may actually follow the fibroblasts.[7] Other co-culture studies have shown that tumor cells recruit macrophages, which in turn produce growth factors and nutrients to permit a more migratory phenotype,[8] and that endothelial cells display enhanced capillary morphogenesis when cultured in the presence of mesenchymal stem cells or fibroblasts.[8,9]

The extracellular microenvironment associated with tumors is vastly different from normal healthy tissues,[10] and it is widely believed this abnormal environment plays an important instructive role in tumor morphogenesis. The loss of normal tissue structure and function observed in most cancers coincides with, and may be causal for, changes in cellular phenotype.[10] The

[a]Department of Biomedical Engineering, University of California, 3410 Natural Sciences II, Irvine, CA, 92697-2715, USA. E-mail: cphuang@uci.edu; Fax: +1 949-824-1727; Tel: +1 949-824-7124

[b]Department of Chemical Engineering and Material Sciences, University of California, 3109 Natural Sciences II, Irvine, CA, 92697-2715, USA. E-mail: njeon@uci.edu; Fax: (+949) 824-1727; Tel: (+949) 824-9032

[c]Department of Pathology and Laboratory Medicine, University of California, Irvine, CA, 92697-2715

[d]School of Mechanical and Aerospace Engineering, Seoul National University, Seoul, 151-744, Republic of Korea

† Electronic supplementary information (ESI) available: Movies S1 and S2. See DOI: 10.1039/b818401a

microenvironment minimally provides sites for integrin-mediated cell attachment, sequesters soluble growth factors and chemokines, and influences diffusive and interstitial transport.[4] Cell attachment to the extracellular matrix (ECM) allows cells to exert tractional forces upon their microenvironment, which in turn is critical for their ability to migrate along and/or through the ECM. Cell-mediated remodeling of the ECM through both force generation and proteolysis is also believed to play a key role in tumor cell invasion and metastatic spread, although there is also evidence that tumor cells can literally squeeze their way through openings in the ECM independent of proteolysis.[11]

To date, most studies of 3D tumor cell invasion involve some variation of a transwell assay.[13–15] These transwell invasion assays, a modification of the Boyden chamber, typically measure cell migration through a 3D gel (typically Matrigel) into a filter under the influence of a chemoattractant. These assay systems are available commercially, but do not provide a real-time assessment of the cell activity in the 3D environment. Furthermore, despite insights gleaned from these and other studies employing 3D cultures, most systems typically lack the ability to spatially pattern multiple cell types in 3D in a consistent manner. To solve these issues, many groups have turned to microfluidic systems, which allow the patterning of cells in specific configurations[3,16–18] and allow precise control over cell–cell or cell–matrix interactions. They also allow the incorporation of biomaterial hydrogels (either natural or synthetic) to create 3D environments.[16,19–22] However, past microfluidic devices either required extensive pumping systems to pattern gels,[12] complicated fabrication processes involving etching of substrates,[13] syringe micromanipulators,[15,16] or complex polymers to confine the hydrogel in a specific channel.[14] These devices require experimental setups and equipment not readily available in most labs. In addition, the forces involved in containment of the hydrogels within these microfluidic devices have not been adequately characterized and/or modeled.

To address these limitations and to better mimic the complex nature of the microenvironment, here we present a new microfluidic device that allows the precise patterning of 3D biopolymer gels into distinct layers. Key features of this microfluidic environment are the ability to observe cell–ECM and cell–cell interactions in 3D in real-time, and to engineer precise structures with well-defined geometries. In addition, we developed a quantitative model to predict the process of filling the microfluidic system with biopolymer gel precursor solutions in order to better understand how the gels are fabricated and constrained by the design specifications of our system. We demonstrate the utility of this device to systematically investigate multiple cell types and multiple ECM substrates in a controlled microenvironment. Combined with our prior work demonstrating the ability to apply gradients across these 3D environments,[15] this integrated platform allows for the study of multicellular morphogenic processes in a dynamic microenvironment.

Results and discussion

Device design and fabrication

This paper describes a novel microfluidic platform that was designed to permit patterning of gels and cells in a 3D microenvironment. Although a number of approaches have been described for patterning cells on 2D surfaces, it has been a challenge to embed multiple cell types in a precisely controlled manner in 3D gels. We recently described an approach to pattern microscale gels within a microfluidic device and generate gradients under flow-free conditions.[15,16] The system described here advances the capability to pattern multiple gels reliably. Similar to our prior "ladder chamber" device,[15,16] the basic design of the device consists of two parallel channels that are connected to reservoirs, but with important modifications that allow different gels to be placed in precise spatial orientations. Instead of a series of narrow microchannels, the main channels were separated by a series of juxtaposed channels partitioned by linear arrays of regularly spaced posts. Using this design, the multiple channels can be independently filled with distinct hydrogels, either through thermally or photo-crosslinked polymerization. Gel composition and dimensions can be engineered for specific applications.

The basic design of the device with a single gel channel configuration is shown schematically in Fig. 1a and movie S1†. The top view and cross-sectional view illustrate the three main structural components of the device: a gel channel (pink), two main channels (blue), and an array of post structures (white) separate them. The design of the device can be readily adapted to include multiple gel channels that can be independently and sequentially filled with gels of desired mechanical and chemical properties. The gel channel (highlighted in pink) can also be designed with varying dimensions. We have successfully tested channels with widths from 100–1000 μm and heights of 50–300 μm. The gel channel is flanked by main channels that act as media and growth factor reservoirs (highlighted in blue). Each gel channel is partitioned using a series of regularly spaced posts that are 50–100 μm apart. Cylindrical and hexagonal posts with diameters ranging from 50–100 μm were used. The purpose of the post structures is to separate gel compartments and prevent leakage into neighboring channels. Instead of a solid barrier that would prevent diffusion and movement of molecules and cells, the use of post structures allows better control of the interface between gel compartments and main channels (interface area can be varied according to need). Using this approach, it is possible to associate (independent) gels with controlled dimensions.

Successful filling of the gels depends on balancing the capillary forces and surface tension within the microfluidic gel channel. If the surfaces within the channel were hydrophilic, we found that the gel or fluid leaked into adjacent channels as soon as the fluid was injected. However, if the surfaces within the channel were hydrophobic, the entire length of the gel channel ($\geq$2 cm in our experiments) could be filled without leakage (see movie S1†). A simple two-step process was applied to generate multiple juxtaposed gels, in which cell-laden gels are formed by filling alternate gel channels followed by polymerization in the first step, with subsequent filling of the remaining channels in the second step (Fig. 1b). These two steps can be achieved by simply filling the gel channels with a pipette in order to produce well-defined 3D gels that are spatially patterned. Alternatively, a syringe pump can be used to infuse gels in a more controlled manner if desired. Importantly, the versatility of our design and fabrication processes allow for the dimensions of each individual gel channel to be tailored, and for each to contain a distinct biomaterial. This may be particularly useful to address specific biological questions regarding the spatial orientation of one cell population with
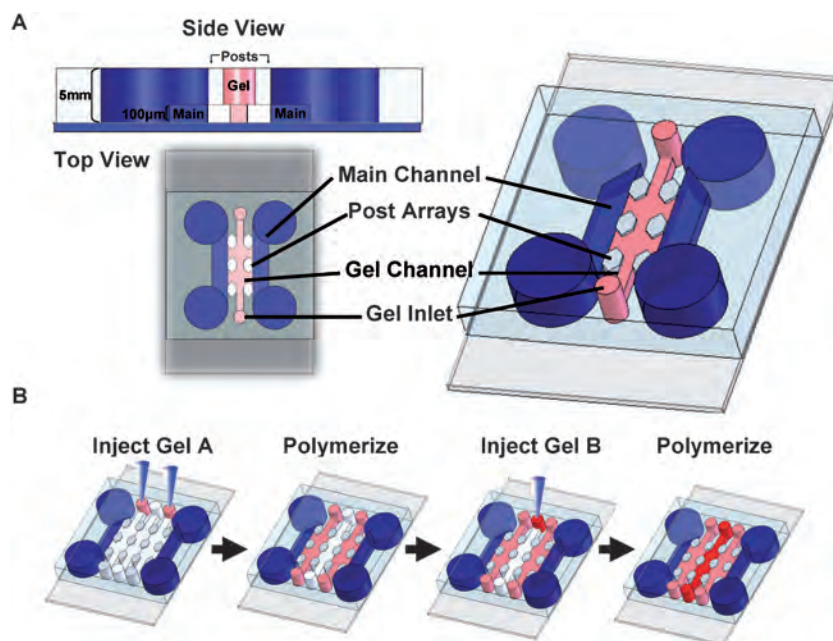
Fig. 1 (A) Device schematic of a single channel device. Two parallel reservoir channels provide media and nutrients to the gel channels contained between them. Arrays of hexagonal posts provide support and contain the gels during the injection process. Each post is 100 μm in diameter and each gel channel is 400 μm across. (B) Gel suspensions can be injected into the inlets *via* manual pipetting or syringe pumps. Filling multichannel devices involves injecting hydrogels in alternating channels, polymerizing, and repeating for remaining channels.

respect to another, or the interface separating one matrix from another. Such control could be useful, for example, to facilitate a better understanding of the roles of soluble diffusible factors in the interactions between tumor cells and their surrounding stromal environment. Ultimately, these approaches may enable construction of custom microenvironments for multicellular co-cultures, the microscale equivalent of master-planned communities.

The effects of surface tension and injection pressures on gel entrapment

Currently there are a variety of microfluidic devices that are being used to study 3D behavior of cells.[12–14,17–19] A distinction of our system is the presence of the interface between juxtaposed gel channels, a critical feature to permit cell–cell and/or cell–gel interactions between adjacent compartments. Creation of this interface was made possible by a series of regularly spaced posts, which function as geometric capillary burst valves.[20] We used hexagonal posts to assure that the interfaces were pinned between the designated vertices as explained below. In the following, we describe how the posts prevent liquid from leaking into adjacent channels since this feature underlies the central working principle of our system. Creation of this interface was made possible by a series of regularly spaced posts (50–100 μm diameter), and empirically found to depend on three different variables: the spacing between posts, the surface properties of the device, and the viscosity of the hydrogel precursor solutions. With respect to these three variables, we first systematically tested various gap spacings (ranging from 50–200 μm) to optimize this interface so that the structural integrity of the gels within each individual gel channel was maintained (*i.e.*, there was

no leakage between adjacent channels). Gap spacings up to 200 μm were found to contain gels within a 400 μm wide gel channel. Second, the surface properties of the device were equally important to prevent the gels from leaking into neighboring channels. When the surfaces of the gel channels were made relatively hydrophobic, the gel precursor solutions did not cross the boundary defined by the posts, thus maintaining the integrity of the resulting gels. If the devices were left hydrophilic, the hydrogels would not be reliably contained within their designated channels and escape into adjacent regions. Finally, hydrogel viscosity was also found to play a crucial role in optimizing the interface between gel channels, with higher density hydrogels exhibiting higher viscosity and displaying an increased chance of leakage between adjacent channels. Collagen gels up to 6 mg mL^{-1} were successfully filled into the system with minimal leakage (<30%), while 8 mg mL^{-1} collagen gels could not be injected reliably without compromising the integrity of the interface. Matrigel concentrations of 8 mg mL^{-1} were also observed to induce leakage into adjacent compartments with a high probability (>80%), while 6 mg mL^{-1} concentrations generated minimal leakages (<10%). Fibrin precursor solutions with concentrations up to 20 mg mL^{-1} could also be injected and polymerized within the device (data not shown). These observations indicate that hydrogels of various identities and densities are compatible with our platform.

To better understand our empirical observations and determine the critical factors that affect the success of the gel filling process within the channels of our device, a modified capillary burst valve model[20] was introduced and adapted to our system to investigate the effects of different geometric dimensions during the gel filling process. As described in the Experimental section, the model equation describes the pressure drop across the liquid

interface (P_i − P_o) as a function of the surface tension (γ), contact angles of the gel channels (θ_s and θ_v), and the width (w) and height (h) of the gel channels (Fig. 2A–2C). We hypothesized that the pressure differences exerted at the liquid interface are critical in determining if leakage may occur, and that a balance between surface tension forces and capillary forces during the gel injection process is necessary to maintain the integrity of the gel interface between adjacent channels. During the injection process, a pressure difference (ΔP) is created at the interface by the liquid (assumed to be water) which drives the liquid into the channel. As the gel fills the channel and gap spacings, pressure differences are generated at the multiple leading interfaces of the hydrogel. The pressure differences decrease as the interface moves away from the injection site. From this model we would predict that if the pressure differential (ΔP_{gap} − ΔP_{width}) exceeds a minimum threshold, then leakage will not occur. Experimentally, if and when the fluid interface passes the first gap spacing, our model would predict that the above minimum threshold condition was satisfied and thus leakages further down the channel would be rare. It was desirable to determine the channel and post dimensions, *i.e.* w and s (Fig. 2C), such that the difference between ΔP_{width} and ΔP_{gap} was large. ΔP_{width} is the minimum amount of pressure required to drive the liquid to

overcome the pressure drop along the fluid channel, while ΔP_{gap} is the maximum pressure threshold that the system can withstand before leakage occurs. The injection pressure has to be finely tuned so that it lies within the range between ΔP_{gap} and ΔP_{width} and will vary depending on the viscosity of the liquid (which correlates with our observations). For example, in our PDMS channels with h = 50 μm, w = 400 μm, ΔP_{width} = 2480 Pa when the liquid is assumed to be water (γ = 0.072 N m⁻¹ and θ_A = 140°). When the post spacing was s = 100 μm, ΔP_{gap} = 3310 Pa, then the pressure differential, ΔP_{width} − ΔP_{gap} = 830 Pa, which was above the threshold to prevent liquid leakage into adjacent channels while the liquid completely filled the straight channel. However, we experimentally observed that the liquid interface pinned between the posts nearest to the fluid inlet started to burst when the gap spacing (s) increased past 200 μm. In this case, the corresponding ΔP_{gap} = 2750 Pa, which exceeds ΔP_{width} by 270 Pa (∼2 cm H_2O) (Fig. 2D). To provide a consistent threshold for future designs, a differential pressure limit of 500 Pa was set as a guide for designing geometries to maximize the interface between channels and provide containment of hydrogels. Although this model assumes a filling liquid of water, these predictions are consistent with our empirical observation and provide a guide to designing geometries to entrap hydrogels.
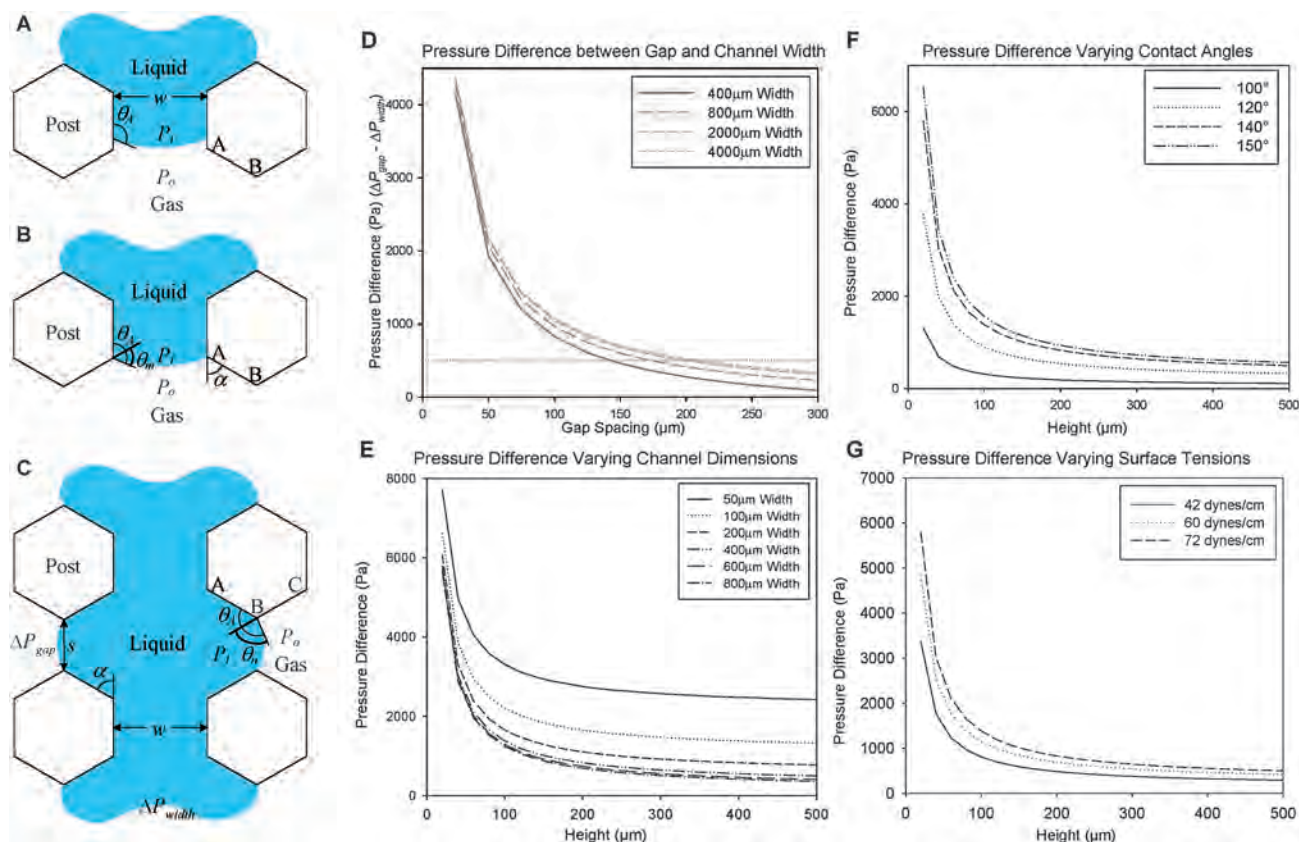

Fig. 2 (A–C) Diagram of a filling process within a channel. During injection, a difference in pressure occurs at the air–liquid interface (ΔP) which depends on surface tension forces (γ), channel geometry (w and s), and contact angles with the wall of the advancing liquid (θ_A). (B) When the liquid interface encounters a gap spacing (point A–B), a new contact angle (θ_m) develops. (C) The difference between the gap spacing (ΔP_{gap}) and channel (ΔP_{width}) need to be maximized to prevent gel leakage. (D–G) Graphs of calculated pressure differences across a variety of parameters: height (E–F), width (E), contact angles (F), and surface tension (G). (D) Graph of pressure differences of increasing gap spacing. A threshold of 500 Pa was set empirically for criteria to prevent leakages and drawn as a guide for reference.

In addition, changes in the surface hydrophobicity (characterized by the contact angle), geometry of the channels will influence the magnitude of the pressure difference. Under hydrophobic conditions (assuming a $\theta_s \approx \theta_v = 140°$ between PDMS and water),[21] and varying the geometries of the channel width and height, we calculated higher pressure differences (Fig. 2E) which scaled linearly if either parameter was changed. As height or width increased from 50–100 μm, the pressure differences dropped drastically but eventually leveled off when past 200 μm. The same trends were observed when plotting with varying contact angles (Fig. 2F) and surface tensions (Fig. 2G). With increasing contact angles from 100° to 150°, higher pressures were calculated which correlates with empirical data that indicates that hydrophobicity promotes gel integrity.

In summary, these modeling results confirm that the magnitude of the surface tension forces can influence the filling process, and will vary with the type and concentration (*i.e.*, the viscosity) of the hydrogel precursor solution. Furthermore, the relative wettability of the PDMS channels, characterized by the contact angle, will also influence the likelihood of maintaining the integrity of the gel channel interfaces within our device. In general terms, if the pressure difference of the liquid interfaces between the channel and gap spacing is minimal (<∼250 Pa), then the gel precursor solution will leak into the neighboring channels. Therefore, while several other studies have reported similar designs to create 3D cell cultures within microfluidic devices,[12,16–19] the combination of experimental data and simulation presented here provides a unique fundamental perspective to understand the rationale behind the operation of this microfluidic platform.

Patterning juxtaposed gels of distinct ECM compositions

To demonstrate the capability to spatially pattern distinct and separate gels, type I collagen and Matrigel were used to fill multiple adjacent channels (Fig. 3, top and bottom rows). Initially, 4 mg mL^{-1} type I collagen hydrogels were mixed with FITC and patterned within a 5-gel channel device to demonstrate that the gel could be contained within single channels without leakage into adjacent channels (Fig. 3, top). The collagen-filled channels are highlighted in green whereas the empty adjacent channels are in black. These data illustrate that the gels were entrapped in separate compartments and did not leak into neighboring channels. Each of the gel channels and gap spacings were filled in a homogenous fashion and created uniform 100 μm boundaries between adjacent gel channels. Using this technique, precursor solutions of collagen type I, Matrigel, or fibrin were also successfully infused into the device and polymerized in adjacent channels for subsequent experiments. Type I collagen gels (4 mg ml^{-1}) polymerized adjacent to Matrigel (4 mg ml^{-1}) in a 5-gel channel device could be easily distinguished from the Matrigel channels by the fibrillar nature of the collagen. Patterning different hydrogels in adjacent gel channels in this fashion demonstrates that the formation of multi-layered microenvironments within our versatile device is straightforward and relatively simple, without the need for complicated materials, pumps, or other equipment. Such multi-layered environments may yield new insights regarding how the migration and invasion of cells in 3D changes as they encounter different ECM ligands and different soluble cues sequestered within the different ECM layers.
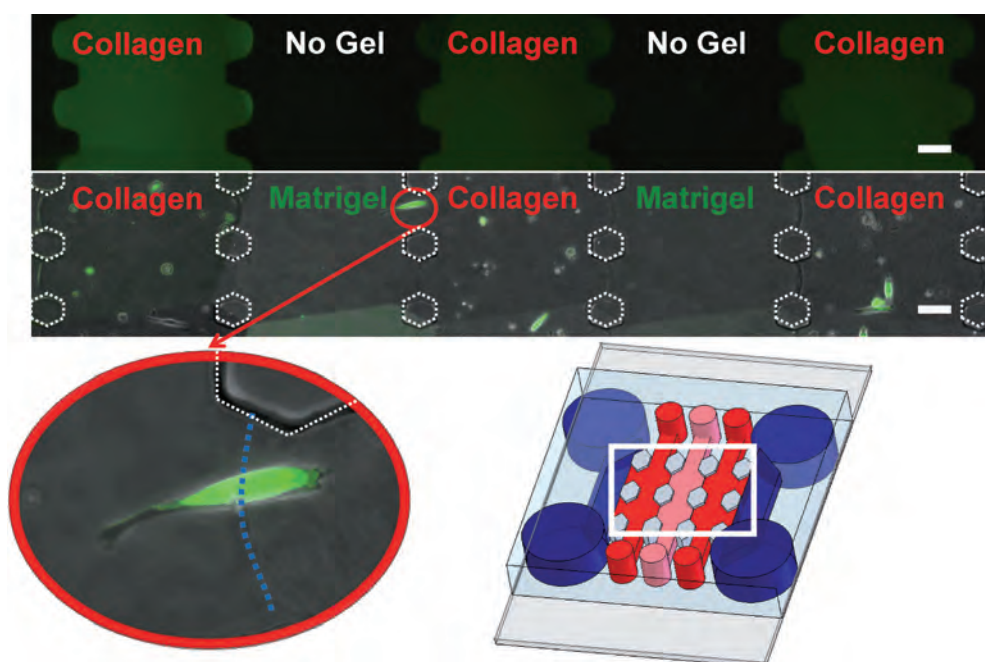

Fig. 3 Collagen gels with FITC dye were patterned in alternating gel channels to show the ability to pattern separate distinct channels without any leakage (top row). Collagen and Matrigel hydrogels (each 4 mg ml^1) were polymerized in alternating gel channels (bottom row). GFP tagged MDA-MB-231 cells were suspended in the collagen and cultured for up to two weeks. Shown is a combined phase and fluorescent micrograph taken at day 6. The magnified insert shows a cell crossing the boundary of the Matrigel–collagen interface. Each gel channel can be patterned independently. Scale bars are 100 μm.

To demonstrate the validity of this system for cell culture applications, MDA-MB-231 cells (a metastatic breast cancer cell line), stably expressing GFP, was suspended in the collagen gels (Fig. 3 bottom row). These cells were observed for up to one week within the devices, and largely remained confined within the collagen gel channels for the duration of the experiment. In one case, a single cell was observed to cross the collagen–Matrigel boundary (Fig. 3, inset) only to return to the collagen gel the following day (not shown). This illustrates the utility of this device to perform live-cell imaging on single cells as they navigate across different microenvironments, and indicates that the interfaces between gels are permeable to cells and soluble factors. Cancer cells are known to have unique extracellular environments which differ from normal pathologies,[2,10] and the extracellular environment plays a role in the migratory behavior and invasiveness.[12,15] Using the methods and systems we have developed here, we can now construct different microscale cellular niches for cellular studies using a variety of ECM materials and thereby explore how tumor cell behavior depends on microscale architecture and matrix identity in 3D.

Second Harmonic Generation (SHG) imaging of collagen remodeling

Like most cells, the ability of cancer cells to migrate through 3D environments is likely to depend on their ability to exert tractional forces. It has also been presumed for some time that tumor cells use a battery of proteases to degrade the 3D ECM in order to migrate through it. However, recent evidence suggests that may adopt an amoeboid morphology to slip through the pores present within the ECM network.[15] Thus, to better understand the dynamic nature of the 3D microenvironment surrounding cells, it is also important to observe how the cells remodel their environment. To observe the cell–matrix interface, DS-red labeled MDA-MB-231 cells were suspended in type I collagen (2 mg mL^{-1}) and visualized *via* two-photon microscopy, with the second harmonic generation signals used to visualize the collagen fibrils (highlighted in blue). In an experiment in which two different adjoined collagen gels were observed, an acellular gel remained intact while a gel channel containing the MDA-MB-
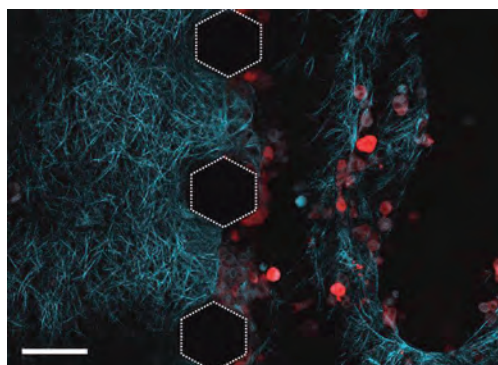

Fig. 4 Collagen fibers were imaged *via* Second Harmonic Generation (SHG) within a device. DS-Red labeled MDA-MB-231 cells were suspended in type I collagen and placed adjacent to another layer of collagen gel. Matrix degradation and remodeling are observed as cells cluster at the boundary of the gels shown in the image. Scale bar represents 100 μm.

231 cells displayed empty areas devoid of collagen fibrils (Fig. 4). As expected, seeding cells at higher densities increased the degradation and remodeling of the collagen matrix compared to lower cell seeding densities (data not shown). These data show that the MDA-MB-231 cells likely remodeled the collagen matrix through a combination of proteolysis and tractional stress (see movie S2†), both of which will depend on the cell density and the ECM density.

Constructing multicellular niches for real-time observation of co-cultures

The tumor microenvironment is complex, and recreating it for *in vitro* studies is a daunting task. Besides the complexities imposed by a 3D microenvironment, cancer cells also interact with a variety of cell types as they grow and metastasize in physiological conditions. For example, recent work has shown that cancer cells actively recruit fibroblasts and macrophages to remodel and produce growth factors to enable the cancer cells to be more invasive.[2,7,8] By dissecting the tumor microenvironment into discrete, well-defined compartments, our system offers a viable strategy to understand the complexities. To show the versatility of the system for potential multicellular culture studies, DS-Red labeled MDA-MB-231 cells and GFP-labeled RAW macrophages (a tumor-associated macrophage cell line) were suspended in collagen (4 mg mL^{-1}) and Matrigel (4 mg mL^{-1}), respectively, and polymerized within the gel channels. Over a one-week time course, the MDA-MB-231 cells (in red) did not invade the neighboring gels, which contained the RAW cells (green) (Fig. 5a). Instead, the RAW cells invaded into the neighboring gels containing the breast cancer cells beginning at day 3. [RAW cells were less invasive into the neighboring gels when MDA-MB-231 cells were not present ($n = 3$) (Fig. 5b).] The invasion of the RAW cells was more extensive after 7 days. RAW cells also appeared to multiply in the presence of MDA-MB-231 cells. These observations may represent a normal macrophage response in which the presence of the foreign tumor cells mobilizes the RAW cells. Alternatively, the MDA-MB-231 cells may also secrete soluble chemoattractant factors that induce the macrophages to proliferate and invade. Further investigation of these phenomena in the system we have described here could therefore potentially provide an improved mechanistic understanding of the interactions between tumor cells and stromal cells in their 3D microenvironment. While such details are beyond the scope of this current work, the system described here nevertheless offers the potential to study the relative contributions of these effects in a systematic and reasonably high-throughput manner.

Experimental

Fabrication and preparation of the device

Silicon wafers (Silicon Inc., Boise, ID) were coated with SU-8 (MicroChem, Newton MA) to generate master molds with 50 μm or 100 μm heights. The wafers were baked at 65 °C and then 95 °C to evaporate any solvent, leaving only the epoxy resin and photo acid generator. When exposed to UV light, an acid reaction occurred which cross-links the epoxy resins to form the patterned structures. The SU-8 was then baked at 95 °C. PDMS (polydimethyl siloxane) was then cast on this mold, cured at 65 °C, and then cut out with appropriately sized holes punched out using cylindrical biopsy
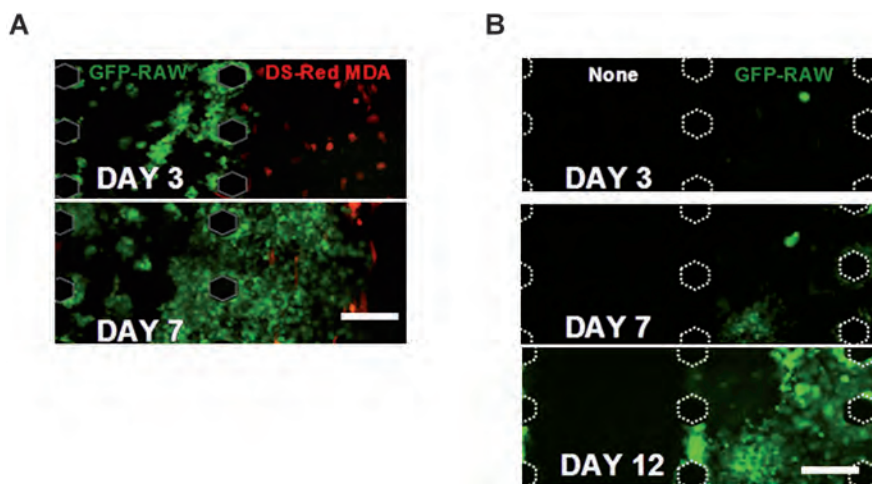
Fig. 5 (A) A co-culture system consisting of 4 mg mL^{-1} collagen containing DS-red-labeled MDA-MB-231 patterned adjacent to 4 mg mL^1 Matrigel containing GFP-labeled RAW cells demonstrates the potential of the system to pattern multilayers of gels as well as multiple cell types. (B) GFP labeled RAW cells were cultured independently from MDA-MB-231 cells in a multi-gel channel device and observed for over 12 days. Scale bars are 200 µm.

punches of various sizes. The devices, along with #2 cover glass slips, were then plasma treated for 5 min using an oxygen plasma generator (Harrick Plasma, NY). The PDMS devices and the glass cover slips were then bonded together irreversibly. To minimize gel leakage from the devices, they were incubated in an oven set at 100 °C for 1–2 hours. The devices were then UV treated for 15 min to sterilize prior to cell culture applications.

Gel fabrication and injection protocols

High concentration rat tail type I collagen was purchased from BD Biosciences (Cat #354249). To make gel precursor solutions, the collagen stock (solubilized in 0.02 N acetic acid) was diluted in ddH$_2$O, 0.1N NaOH, and 5x DMEM media. Different concentrations of collagen were made by adjusting the amount of collagen and adding the appropriate amount of 0.1N NaOH (to neutralize the acetic acid). The solution was then placed on ice to impede the polymerization and allow time to prepare the cells along with the devices. High concentration Matrigel was purchased from BD Biosciences (Cat #354248). Gels of 4 mg mL^{-1} Matrigel concentrations were prepared by diluting the Matrigel stock with DMEM.

Suspensions of cells were mixed with collagen or Matrigel solutions and then carefully injected (10 µL total volume) into each PDMS device using a P20 pipetteman. The devices were then left in the cell culture hood for 20 min to 1 h to allow for *in situ* polymerization. After the gel polymerized, media was added to the inlet reservoirs of the device and gently suctioned using a glass micropipette attached to a house vacuum. The device was then placed in a Petri dish to maintain sterility and transferred to a 37 °C incubator.

Co-culture and multi-channel experiments

MDA-MB-231 was purchased through ATCC. (#HTB-26) and transfected with GFP using Lipofectamine 2000 (Invitrogen). DS-red labeled MDA-MB-231 cells and GFP labeled RAW 264.1 macrophages were obtained as a gift from the Klemke lab (UCSD). All cells were cultured in DMEM with high glucose (Sigma-Aldrich) supplemented with 10% (v/v) fetal bovine serum

(Gibco) at 37 °C in a 5% CO$_2$ humid incubator. For the multigel experiments, a 5-gel multichannel device was used to pattern the different hydrogels. GFP labeled MDA-MB-231 cells (2.5×10^5) were suspended in 100 µL of 4 mg mL^{-1} collagen and then injected into alternating gel channels and polymerized at 37 °C for 40 min. Matrigel (100 µL of 4 mg mL^{-1}) was then injected into the two remaining channels and polymerized at 37 °C for 40 min. Media was then flowed into the main channels and the device was cultured in an incubator at 37 °C with 5% CO$_2$. The media was changed every other day before image acquisition.

For co-culture experiments, a 5-gel multichannel device was employed. DS-red labeled MDA-MB-231 cells (2.5×10^5) were suspended in 100 µL of 4 mg mL^{-1} collagen precursor solution and then injected into the three alternating gel channels. Devices were then incubated at 37 °C for 40 min to allow for gel polymerization. GFP labeled RAW cells (2.5×10^5) were then suspended in 100 µl of 4 mg mL^{-1} Matrigel and injected into the remaining channels. The device was incubated at 37 °C for another 40 min to ensure the Matrigel solidified before filling the main channels with media.

Fluorescent and phase micrograph images were acquired every two days using an Olympus 1X-51 inverted microscope. Multigel and co-culture experiments were captured at 10X magnification using a Q-Imaging QICAM 12 bit Color Fast 1394 camera (QImaging, Surrey, BC) and Qcapture Pro (QImaging, BC, Canada) imaging software. The images were then stitched and merged using ImageJ (NIH) and Adobe Photoshop (Adobe Systems Inc., CA).

Multiphoton microscopy

Second harmonic generation (SHG) and two photon fluorescence (TPF) images used to visualize the collagen matrix and cells were imaged on a Zeiss LSM510 meta multiphoton system (Jena, Germany) as previously described.[22] Images generated using 543 nm and 800 nm excitation wavelengths were visualized with a 40X Achroplan 0.8 numerical aperture water immersion objective (Zeiss). Z-stacks were compiled by imaging 1–2 µm

thick optical sections. Each 12 bit image consists of a 225 × 225 μm² area and pinhole size and laser power were kept constant throughout the imaging. A 675 μm × 1350 μm montage was generated by stitching the acquired images.

A triple-gel channel device was prepared by polymerizing a 2 mg mL⁻¹ collagen suspension containing 2.5×10^4 DS-Red MDA-MB-231 cells in the center gel channel. Adjacent channels were then filled and polymerized with 2 mg mL⁻¹ collagen. The device was cultured in growth media and imaged on the third day. Areas surrounding the interface between the acellular and cell containing collagen were imaged at 40X. Fibers were highlighted by back scattering of the second harmonic signal while the cells were fluorescently excited.

Capillary burst valve injection model

To understand the physical basis of our gel filling process and the forces generated on the gap spacings, a two dimensional model of a single gel channel within the device was constructed from a modified capillary burst valve. We assume the critical point during the gel injection occurs when the gel front approaches the first gap spacing between post structures. To simplify the calculations as the hydrogel solution approaches, a single channel with hexagonal posts and gap spacings of 100 μm was created. When an advancing liquid interface meets the straight section of the posts at equilibrium (Fig. 2a), the difference between the pressure inside the liquid P_i and atmospheric pressure P_o is given by the Young–Laplace equation (which states that the pressure drop is a function of the surface tension γ and the interface curvature), $P_i - P_o = -2\gamma(\cos\theta_s/w + \cos\theta_v/h)$, where w and h are the width and the height of the channel, respectively, θ_s is the advancing contact angle formed between the liquid interface and the side wall, and θ_v is the advancing contact angle of the liquid with the top and bottom walls. Here it should be noted that the liquid interface can only move forward when the contact angles with the solid walls exceed the critical advancing contact angle, θ_A, which is determined by the liquid/solid combination. When the contact line speed is sufficiently low that the capillary number, $C_a = \mu U/\gamma < 1 \times 10^{-3}$, where μ is the liquid viscosity and U is the contact line velocity, we may set $\theta_s \approx \theta_v \approx \theta_A$. When the interface meets the edge A of the post as in Fig. 2b, the contact angle with a new wall (A–B) is reduced to $\theta_m = \theta_A - \alpha$, where $\alpha = 60°$, which causes the contact line to stop because $\theta_m < \theta_A$. For the contact line to resume advancing, the interface should bulge until the contact angle with the new wall increases to θ_A, leading to the increase of the contact angle with the old wall (before A) from θ_A to $\min\{\theta_A + \alpha, 180°\}$ (The contact angle never exceeds 180°). Therefore, for the liquid interface to move beyond the point A, the driving pressure difference $P_i - P_o$ should be greater than $\Delta P_1 = -2\gamma(\cos\theta_1/w + \cos\theta_A/h)$, where $\theta_1 = \min\{\theta_A + \alpha, 180°\}$. Assuming that a sufficient pressure is supplied to overcome the foregoing barrier A, the liquid fills the straight channel until its interface meets a new wall (B–C) with which it makes a new contact angle $\theta_n = \theta_A - \alpha$, as shown in Fig. 2c. Unless the driving pressure increases to bulge the interface till θ_n reaches θ_A, the liquid interface is pinned at B. The critical pressure causing the interface pinned at B to resume advancing (or the liquid to leak into adjacent channels) is again given by the Young–Laplace equation, $\Delta P_2 = -2\gamma(\cos\theta_2/s + \cos\theta_A/h)$, where $\theta_2 = \min\{\theta_A + \alpha, 180°\}$. Stopping the liquid

interface at B, where the diverging section begins, is the major role of the posts at the geometric capillary burst valve. It should be noted that the interface pinning location is precisely determined by hexagonal posts (between nearest vertexes of neighboring posts) while the rectangular posts as previously used are unable to guarantee pinning of the liquid interface at pre-defined locations.[17]

Conclusions

This paper describes an approach to engineer 3D microenvironments for investigating cell–cell and cell–ECM interactions using a microfluidic platform. This approach is based on a set of parallel microfluidic channels separated by an array of posts that allow selective filling of individual channels, yet permits continuous interfaces between adjacent channels for free diffusion of molecules as well as movement of cells across distinct regions. The advantages of this system when compared to current models presently available are: (i) it allows the patterning of different combinations of hydrogels and culturing of multiple cell types in a relatively easy and straightforward manner, (ii) it can be scaled dimensionally to mimic multicellular *in vivo* structures, and (iii) it can be used to generate chemically and mechanically tailored 3D cellular niches in a reproducible manner. We successfully patterned adjacent channels filled with ECM hydrogels (collagen, fibrin, Matrigel) of various concentrations to create distinct layers of different composition with a range of dimensions (100–300 μm in height, 100–400 μm in width). We also provided a simulation model to better understand the mechanics of the injection process. Finally, the utility of this system for multicellular 3D cultures was demonstrated by investigating the behaviors of metastatic breast cancer cells and tumor-derived macrophages in spatially well-defined geometries. In these experiments, distinct phenotypes were exhibited by the macrophages when cultured next to the tumor cells, possibly due to paracrine signals that diffuse between adjacent gel channels. In future studies, this system will enable these paracrine effects on normal and tumor cell functions to be investigated further, in concert with changes in ECM ligand identity and density and gradients of soluble diffusible factors.

Acknowledgements

References

1 C. Fischbach, R. Chen, T. Matsumoto, T. Schmelzle, J. S. Brugge, P. J. Polverini and D. J. Mooney, *Nat. Methods*, 2007, **4**, 855–860.
2 K. M. Yamada and E. Cukierman, *Cell*, 2007, **130**, 601–610.
3 D. R. Albrecht, G. H. Underhill, T. B. Wassermann, R. L. Sah and S. N. Bhatia, *Nat. Methods*, 2006, **3**, 369–375.
4 L. G. Griffith and M. A. Swartz, *Nat. Rev. Mol. Cell Biol.*, 2006, **7**, 211–224.
5 R. N. Bhandari, L. A. Riccalton, A. L. Lewis, J. R. Fry, A. H. Hammond, S. J. Tendler and K. M. Shakesheff, *Tissue Eng.*, 2001, **7**, 345–357.
6 A. Khademhosseini, L. Ferreira, J. Blumling, 3rd, J. Yeh, J. M. Karp, J. Fukuda and R. Langer, *Biomaterials*, 2006, **27**, 5968–5977.
7 C. Gaggioli, S. Hooper, C. Hidalgo-Carcedo, R. Grosse, J. F. Marshall, K. Harrington and E. Sahai, *Nat. Cell Biol.*, 2007, **9**, 1392–1400.
8 C. M. Ghajar, X. Chen, J. W. Harris, V. Suresh, C. C. Hughes, N. L. Jeon, A. J. Putnam and S. C. George, *Biophys. J.*, 2008, **94**, 1930–1941.
9 C. M. Ghajar, K. S. Blevins, C. C. Hughes, S. C. George and A. J. Putnam, *Tissue Eng.*, 2006, **12**, 2875–2888.
10 C. M. Nelson and M. J. Bissell, *Annu. Rev. Cell Dev. Biol.*, 2006, **22**, 287–309.
11 K. Wolf, R. Muller, S. Borgmann, E. B. Brocker and P. Friedl, *Blood*, 2003, **102**, 3262–3269.
12 Y. C. Toh, C. Zhang, J. Zhang, Y. M. Khong, S. Chang, V. D. Samper, D. van Noort, D. W. Hutmacher and H. Yu, *Lab Chip*, 2007, **7**, 302–309.
13 T. Frisk, S. Rydholm, T. Liebmann, H. A. Svahn, G. Stemme and H. Brismar, *Electrophoresis*, 2007, **28**, 4705–4712.
14 A. P. Wong, R. Perez-Castillejos, J. Christopher Love and G. M. Whitesides, *Biomaterials*, 2008, **29**, 1853–1861.
15 B. Mosadegh, C. Huang, J. W. Park, H. S. Shin, B. G. Chung, S. K. Hwang, K. H. Lee, H. J. Kim, J. Brody and N. L. Jeon, *Langmuir*, 2007, **23**, 10910–10912.
16 W. Saadi, S. W. Rhee, F. Lin, B. Vahidi, B. G. Chung and N. L. Jeon, *Biomed Microdevices*, 2007, **9**, 627–635.
17 S. Chung, R. Sudo, P. J. Mack, C. R. Wan, V. Vickerman and R. D. Kamm, *Lab Chip*, 2009, **9**, 269–275.
18 C. P. Ng and S. H. Pun, *Biotechnol Bioeng*, 2008, **99**, 1490–1501.
19 V. Vickerman, J. Blundo, S. Chung and R. Kamm, *Lab Chip*, 2008, **8**, 1468–1477.
20 H. Cho, H. Y. Kim, J. Y. Kang and T. S. Kim, *J. Colloid Interface Sci.*, 2007, **306**, 379–385.
21 T. Engländer, *J. Colloid Interface Sci.*, 1996, **179**, 635–636.
22 C. B. Raub, V. Suresh, T. Krasieva, J. Lyubovitsky, J. D. Mih, A. J. Putnam, B. J. Tromberg and S. C. George, *Biophys. J.*, 2007, **92**, 2212–2222.